ACS APPLIED MATERIALS & INTERFACES

Research Article

www.acsami.org

Photoinduced Smart, Self-Healing Polymer Sealant for Photovoltaics

Sanjib Banerjee,[†] Ranjan Tripathy,[†] David Cozzens,[†] Tibor Nagy,[‡] Sandor Keki,[‡] Miklos Zsuga,[‡] and Rudolf Faust*,[†]

[†]Department of Chemistry, University of Massachusetts Lowell, One University Avenue, Lowell, Massachusetts 01854, United States

[‡]Department of Applied Chemistry, University of Debrecen, Egyetem ter 1, Debrecen H-4032, Hungary

Supporting Information

ABSTRACT: Polyisobutylene (PIB)-based polymer networks potentially useful as smart coatings for photovoltaic devices have been developed. Low molecular weight coumarin functional triarm star PIB was synthesized via a single step S_N2 reaction of bromoallyl functional triarm star PIB with 4-methylumbelliferone or umbelliferone in the presence of sodium hydride. Quantitative end functionality was confirmed by matrix-assisted laser desorption/ionization time-of-flight mass spectrometry. UVA (λ_{max} = 365 nm) induced reversible photodimerization of the coumarin moieties resulted in cross-linked elastomeric films exhibiting self-healing behavior. The extent of photodimerization/photoscission was monitored by UV−vis spectroscopy. The low oxygen (1.9×10^{-16} mol m m^{-2} s^{-1} Pa^{-1}) and moisture (46×10^{-16} mol m m^{-2} s^{-1} Pa^{-1}) permeability of the cross-linked polymer films suggest excellent barrier properties of the cross-linked polymer films. The self-healing process was studied by atomic force microscopy (AFM). For this, mechanical cuts were introduced in the cross-linked PIB films through micromachining with an AFM tip and the rate of healing induced by UV, sunlight, or both was followed by taking AFM images of the film at different time intervals during the repair process.

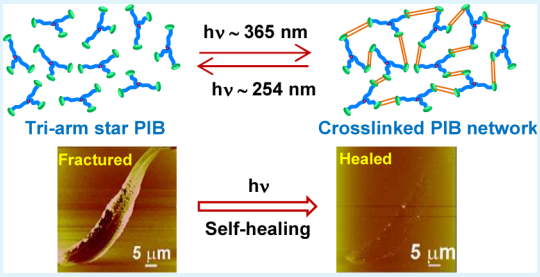

KEYWORDS: *polyisobutylene, photochemistry, self-healing, functional coatings, photovoltaic devices*

INTRODUCTION

Because virtually all materials are susceptible to degradation, self-healing is of great interest to extend the lifetime of materials. The ultimate goal in designing self-healing materials is to achieve healing not only at the microscopic level but also at the nanoscopic level. This is required to arrest crack propagation (which might lead to macroscopic changes in the material), to prevent catastrophic system failure, and to restore all the properties of the material. While there are many examples of self-healing in nature, generally it is difficult to translate these into engineered materials. The first application of autonomic self-healing was reported by White and his collaborators, who first reported self-healing without an external trigger using a microencapsulated healing agent that was released upon crack formation leading to the subsequent polymerization of the healing agent.[1] While many improvements were subsequently made by the same group of authors[2,3] and other researchers,[4] a disadvantage of the microcapsule-based self-healing approach is that multiple healing is not possible. Nonautonomic healing requires an external trigger such as optical,[5] thermal,[6,7] electrical,[8,9] or chemical stimuli.[10] However, multiple healing of a microscopic crack is possible. In practice, reversible interactions such as metal-ligand coordination,[11,12] dynamic covalent bonds,[13,14] hydrogen bonding,[15,16] ionic interactions,[17,18] and $\pi-\pi$ stacking interactions[19,20] have been used to heal damage. Reversible photocyclizations are of great commercial importance as a self-healing trigger due to the capability to heal repeated damage at the same position.[21] Moreover, these photoreactions are inexpensive and environmentally friendly. Olefinic compounds such as cinnamic acid, anthracene, thymine, coumarin, and so on undergo [2 + 2] cyclodimerization upon irradiation with ultraviolet (UV) light of wavelength (λ) > 300 nm to form cyclobutane adduct. Upon irradiation with shorter wavelength of light, they revert back to the starting olefins. Researchers have utilized these reversible cyclodimerization reactions to prepare self-healing polymer systems.[22,23] Nagata and co-workers developed shape memory polymers by reversibly photo-cross-linking the pendent coumarin groups of poly(ε-caprolactone),[24] block copolymers composed of ε-caprolactone and L-lactide,[25] and multiblock copolymers based on poly(ε-caprolactone) and poly(L-lactide) segments.[26]

Organic semiconductor based devices,[27] such as organic light emitting devices (OLED), photovoltaic (PV), and organic solar cells[28] have gained substantial attention in recent times. However, these devices are especially susceptible to damage upon extended exposure to hot and humid environmental conditions.[29,30] Rigid or flexible organic polymeric materials such as poly(methyl methacrylate) (PMMA) or PMMA-polyolefin have been used as coatings to support and provide

Received: November 18, 2014
Accepted: December 29, 2014
Published: December 29, 2014

DOI: 10.1021/am508096c
ACS Appl. Mater. Interfaces 2015, 7, 2064−2072

protection to the underlying semiconductor layers.[31,32] These coatings, however, may themselves be susceptible to the formation of cracks or micro scratches upon prolonged exposure to unfavorable environmental conditions. These cracks or micro scratches act as a stress concentrator site, ultimately allowing moisture to pass through the coating and eventually damage the OLED and PV systems. Furthermore, these coating materials are generally too permeable to moisture and oxygen.[33,34] Hence, in order to obtain flexible organic solar cells with long lifetimes that are devoid of micro scratches, it seemed important to develop coating materials with the following properties: (1) a high barrier to water and oxygen, (2) optical transparency, and (3) flexibility, as well as self-healing property.

Polyisobutylene (PIB)-based networks possess excellent flexibility, strong adherence to substrate, good damping and barrier properties, thermal stability, and excellent chemical and solvent resistance.[35,36] The above properties can be utilized effectively for coatings of OLED, PV, and solar cells. The current work describes the development of a self-healing, gas impermeable elastomeric sealant consisting of a cross-linked, transparent polymer network that exhibits photoinduced crack healing. To the best of our knowledge, this is the first example of sunlight-induced self-healing material.

EXPERIMENTAL SECTION

Materials. Isobutylene (IB, Matheson Tri Gas) and methyl chloride (MeCl, Airgas) were dried in the gaseous state by being passed through in-line gas-purifier columns packed with BaO/Drierite and then condensed in a receiver flask at −80 °C before use. Titanium(IV) chloride ($TiCl_4$, Sigma-Aldrich, 99.9%), 2,6-di-*tert*-butylpyridine (DTBP, Aldrich, 97%), 1,3-butadiene (BD, Aldrich, >99%), lithium bromide (LiBr, Aldrich, ≥98%), 4-methylumbelliferone (MUMB, Aldrich, ≥98%), umbelliferone (UMB, Aldrich, 98%), sodium hydride (NaH, Aldrich, 60% dispersion in mineral oil), potassium hydroxide (KOH, Aldrich) and sodium sulfate (Na_2SO_4, Aldrich) were used as received. Tetra-*n*-butylammonium bromide (TBAB, Alfa Aesar, 95%) was used without further purification. 1,3,5-Tricumyl chloride (TCC) was synthesized by hydrochlorination of the corresponding tricumyl alcohol according to a procedure described in the literature.[37]

Hexanes, mixture of isomers (Hex, Sigma-Aldrich, ≥98.5%, ACS reagent) was purified by refluxing over concentrated sulfuric acid for 48 h. It was then washed with aqueous solution of KOH three times followed by washing with distilled water until neutral to pH paper. It was kept over anhydrous Na_2SO_4 overnight at room temperature and finally distilled over CaH_2 under a nitrogen atmosphere twice before use in the polymerization. Tetrahydrofuran (THF, Aldrich, 99%) was dried by refluxing them over benzophenone (99%, Sigma-Aldrich) and Na-metal (99.9%, Sigma-Aldrich) overnight and distilled under N_2 atmosphere before use.

Synthesis of Triarm Star (PIB-Allyl)$_3$-Cl. Triarm star (PIB-Allyl)$_3$-Cl of molecular weight ∼2000, 5000, and 10 000 g mol^{-1} were synthesized by living cationic polymerization of IB followed by end-capping with BD in Hex/MeCl 60/40 (v/v) mixture at −80 °C using the TCC/$TiCl_4$ initiating system in a MBraun MB200MOD stainless steel glovebox (Innovative Technology, Inc.) equipped with a gas purification system (molecular sieves and copper catalyst) under dry nitrogen atmosphere using a modification of a procedure described previously.[38] In a typical experiment, living cationic polymerization of IB was carried out in Hex/MeCl 60/40 (v/v) at −80 °C using these following initial concentrations of reactants: [TCC] = 0.0185 M, [DTBP] = 0.004 M, [IB] = 0.5 M, and [$TiCl_4$] = 0.036 M. In a 500 mL round bottomed flask equipped with an overhead mechanical stirrer, 7.8 mL of IB, 180 μL of DTBP, 112.2 mL of hexane, 1.132 g of TCC, 61.1 mL of MeCl was added, and the mixture was cooled to −80 °C. 7.9 mL $TiCl_4$ was added to 50 mL MeCl to prepare a stock solution of $TiCl_4$ in MeCl. Then, 5 mL of this solution was added to the culture tube to initiate the polymerization. After 60 min of IB polymerization, 5 mL of the reaction mixture was taken out using a dry syringe and quenched with 0.5 mL of prechilled methanol for the characterization of precursory PIB, and to the rest, appropriate amounts of BD (22.2 mmol at −80 °C) was added under stirring. The reaction was continued for another 4 h. After that, the polymerization was terminated by the addition of 5.0 mL of prechilled methanol at −80 °C. The solvent was evaporated and the crude product was dissolved in Hex. It was then added dropwise to methanol under stirring condition and then allowed to settle down. This dissolution/precipitation step was repeated twice more. Methanol was then decanted out, and the polymer was vacuum-dried for 12 h in a vacuum oven at room temperature to remove any residual methanol. Both precursory PIB and triarm star (PIB-Allyl)$_3$-Cl were characterized using SEC (Table S1 and Figure S1, Supporting Information). Structural characterization of triarm star (PIB-Allyl)$_3$-Cl samples were performed by ^{1}H NMR spectroscopy (Figure 1). ^{1}H NMR (500 MHz, CDCl$_3$, 25 °C, TMS): δ = 7.17 ppm (s, 3H, Ar**H** of TCC), 5.81 ppm (m, 1H, $-C\underline{H}{=}C\boldsymbol{H}CH_2Cl$), 5.62 ppm (m, 1H, $-C\boldsymbol{H}{=}C\underline{H}CH_2Cl$), 4.06 ppm (d, 2H, $-C\underline{\boldsymbol{H}}_2Cl$), 1.43 ppm (s, nH, $-C\underline{\boldsymbol{H}}_2C(CH_3)_2-CH_2CH{=}CHCH_2Cl$), and 1.1 ppm (s, nH $-CH_2C(C\underline{\boldsymbol{H}}_3)_2CH_2CH{=}CHCH_2Cl$).

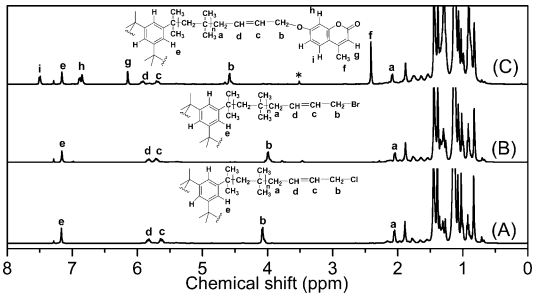

Figure 1. ^{1}H NMR spectra of (PIB-Allyl)$_3$-Cl (A), (PIB-Allyl)$_3$-Br (B) and (PIB-MUMB)$_3$ (C) in $CDCl_3$. (*) Solvent (methanol) peak.

Synthesis of Triarm Star (PIB-Allyl)$_3$-Br. (PIB-Allyl)$_3$-Br was obtained by halogen exchange reaction between (PIB-Allyl)$_3$-Cl and LiBr using a modification of the procedure reported earlier.[39] The reaction was carried out in dry THF using a large excess of anhydrous LiBr with respect to (PIB-Allyl)$_3$-Cl ([LiBr]/[(PIB-Allyl)$_3$-Cl]) = 201) under a dry nitrogen atmosphere. In a typical experiment, (PIB-Allyl)$_3$-Cl ($M_{n,SEC}$ = 2000, M_w/M_n = 1.21, 5.670 g, 2.8 mmol), LiBr (48.880 g, 562.8 mmol) and THF (75 mL) were taken in a two-necked round bottomed flask and refluxed with stirring for 12 h. After that, it was cooled to room temperature, and THF was evaporated under reduced pressure using a rotary evaporator. The crude polymer was dissolved in Hex and taken in a separatory funnel. Excess LiBr was removed by washing with distilled water twice, and the organic layer was dried over anhydrous Na_2SO_4. The polymer was further purified by dissolving in Hex and precipitating in methanol. This dissolution/precipitation cycle was repeated twice more. Methanol was then decanted, and the polymer was vacuum-dried for 12 h in a vacuum oven at room temperature to remove any residual methanol. Structural characterization of triarm star (PIB-Allyl)$_3$-Br samples were performed by ^{1}H NMR spectroscopy (Figure 1). ^{1}H NMR (500 MHz, $CDCl_3$, 25 °C, TMS): δ = 7.17 ppm (s, 3H, Ar**H** of TCC), 5.79 ppm (m, 1H, $-C\underline{H}{=}C\boldsymbol{H}CH_2Br$), 5.68 ppm (m, 1H, $-C\boldsymbol{H}{=}C\underline{H}CH_2Br$), 3.98 ppm (d, 2H, $-C\underline{\boldsymbol{H}}_2Br$), 2.1 ppm (d, 2H, $-C\underline{\boldsymbol{H}}_2CH{=}CHCH_2Br$), 1.43 ppm (s, nH, $-C\underline{\boldsymbol{H}}_2C(CH_3)_2-CH_2CH{=}CHCH_2Br$) and 1.1 ppm (s, nH $-CH_2C(C\underline{\boldsymbol{H}}_3)_2CH_2CH{=}CHCH_2Br$).

Synthesis of Triarm Star (PIB-MUMB)$_3$. Typically, triarm star (PIB-Allyl)$_3$-Br ($M_{n,SEC}$ = 2000, M_w/M_n = 1.21, 5.0 g, 2.5 mmol) was dissolved in dry THF (75 mL) in a two-necked round bottomed flask. Then, MUMB (2.20 g, 125 mmol), TBAB (52.38 g, 162.5 mmol), and NaH (1.8 mg, 75 mmol) were added to it and the mixture was refluxed under a dry nitrogen atmosphere for 12 h. After that, the reaction

DOI: 10.1021/am508096c
ACS Appl. Mater. Interfaces 2015, 7, 2064−2072

mixture was cooled to room temperature. THF was evaporated using a rotary vacuum evaporator, the residue was dissolved in hexanes, and the solution was filtered. The filtrate (polymer solution) was concentrated by evaporation and precipitated in methanol. The polymer was allowed to settle down and the supernatant liquid was decanted. This dissolution/precipitation cycle was repeated twice more. Finally, the polymer was dried under vacuum at room temperature for 12 h. Triarm star $(PIB\text{-}MUMB)_3$ samples were characterized using SEC (Table 1 and Figure S1, Supporting Information). Quantitative end functionality of the triarm star $(PIB\text{-}MUMB)_3$ samples were confirmed by matrix-assisted laser desorption/ionization time-of-flight mass spectrometry (MALDI-TOF MS; Figure 2) and also by electrospray ionization time-of-flight mass spectrometry (ESI-TOF MS) spectrum for $(PIB\text{-}MUMB)_3$-2k (Figure S2, Supporting Information). Structural characterization of triarm star $(PIB\text{-}MUMB)_3$ samples were performed by ^{1}H NMR spectroscopy (Figure 1). ^{1}H NMR (500 MHz, $CDCl_3$, 25 °C, TMS): δ = 7.48 ppm (d, 1H, Ar<u>**H**</u>), 7.13 ppm (s, 3H, Ar<u>**H**</u> of TCC), 6.82 ppm (m, 2H, −Ar<u>**H**</u>), 6.11 ppm (s, 1H, −Ar<u>**H**</u>), 5.89 ppm (m, 1H, −C<u>**H**</u>=CHCH$_2$O−), 5.68 ppm (m, 1H, −CH=C<u>**H**</u>CH$_2$O−), 4.57 ppm (d, 2H, −CHC<u>**H**</u>$_2$O−), 2.39 ppm (s, 1H, −OCOC<u>**H**</u>−), 1.42 ppm (s, nH, −C<u>**H**</u>$_2$C(CH$_3$)$_2$−CH$_2$CH=CHCH$_2$O−) and 1.1 ppm (s, nH −CH$_2$C(C<u>**H**</u>$_3$)$_2$CH$_2$CH=CHCH$_2$O−).

Table 1. Molecular Characterization Data of Triarm Star PIB Samples

sample	$M_{n,NMR}$ [a]	$M_{n,SEC}$ [b]	M_w/M_n [b]	M_n [c]	M_w/M_n [c]
$(PIB\text{-}MUMB)_3$-2k	2360	2100	1.21	2330	1.05
$(PIB\text{-}MUMB)_3$-5k	6490	5200	1.16	4590	1.04
$(PIB\text{-}MUMB)_3$-10k	12180	10700	1.17	– [d]	– [d]

[a] M_n determined from ^{1}H NMR by comparing the integration of the three aromatic protons of the initiator and the aliphatic protons of the polymer. [b] M_n and M_w/M_n values determined by SEC analysis. [c] M_n and M_w/M_n values determined by MALDI-TOF MS for the $(PIB\text{-}MUMB)_3$ samples. Values of M_n and M_w were determined using equations $M_n = \sum M_i I_i / \sum I_i$ and $M_w = \sum M_i^2 I_i / \sum M_i I_i$, where M_i and I_i are the mass and the intensity of the i^{th} oligomer, respectively. [d] Could not be determined.

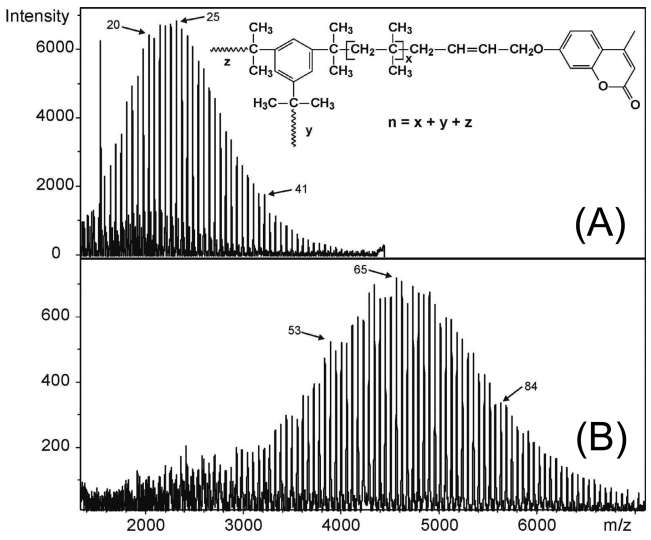

Figure 2. MALDI-TOF MS spectra of (A) $(PIB\text{-}MUMB)_3$-2k and (B) $(PIB\text{-}MUMB)_3$-5k. The numbers with arrows indicate the number of isobutylene units (n).

Synthesis of Triarm Star (PIB-UMB)$_3$. Triarm star $(PIB\text{-}UMB)_3$-2k was synthesized following the same method described above for the synthesis of triarm star $(PIB\text{-}MUMB)_3$. In this case, UMB was used in place of MUMB. M_n and M_w/M_n of $(PIB\text{-}UMB)_3$-2k were determined by SEC (Figure S5, Supporting Information). Structural characterization of triarm star $(PIB\text{-}UMB)_3$ samples were performed by ^{1}H NMR spectroscopy (Figure S6, Supporting Information). ^{1}H NMR (500 MHz, $CDCl_3$, 25 °C, TMS): δ = 7.61 ppm (d, 1H, Ar<u>**H**</u>), 7.36 ppm (d, 1H, Ar<u>**H**</u>), 7.13 ppm (s, 3H, Ar<u>**H**</u> of TCC), 6.83 ppm (m, 2H, −Ar<u>**H**</u>), 6.23 ppm (m, 1H, −Ar<u>**H**</u>), 5.90 ppm (m, 1H, −C<u>**H**</u>=CHCH$_2$O−), 5.67 ppm (m, 1H, −CH=C<u>**H**</u>CH$_2$O−), 4.56 ppm (d, 2H, −CHC<u>**H**</u>$_2$O−), 2.39 ppm (s, 1H, −OCOC<u>**H**</u>−), 1.42 ppm (s, nH, −C<u>**H**</u>$_2$C(CH$_3$)$_2$−CH$_2$CH=CHCH$_2$O−) and 1.1 ppm (s, nH −CH$_2$C(C<u>**H**</u>$_3$)$_2$CH$_2$CH=CHCH$_2$O−).

Procedure for Photodimerization/Photocleavage Study. A 2 wt % solution of $(PIB\text{-}MUMB)_3$ or $(PIB\text{-}UMB)_3$ in THF was prepared by dissolving 20 mg of the polymer in 1.0 mL of the solvent. The solution was filtered through 0.45 μm pore size filter paper to obtain a clear homogeneous solution. It was then drop casted on a clean glass slide. The solvent was allowed to evaporate at room temperature, and the sample was finally dried under vacuum at room temperature in the dark for 12 h to remove traces of THF prior to analysis. The photodimerization reaction of polymer films were carried out at room temperature by irradiating the $(PIB\text{-}MUMB)_3$ or $(PIB\text{-}UMB)_3$ samples using a 400 W high-pressure mercury lamp (Uvitron International, Inc., PORTA-RAY 400 R) at λ_{max} = 365 nm (UVA irradiation). The photocleavage was accomplished by irradiation at λ_{max} = 254 nm (UVC irradiation) using a 400 W medium pressure visible lamp from Uvitron International, Inc. The thin films of the polymer samples on a clean glass slide were placed at a distance of 15 cm below the lamp. The extent of photodimerization/photocleavage was monitored by UV−vis spectroscopy. A gradual decrease and increase of absorbance of coumarin moiety at 320 nm with time was observed during photodimerization and photocleavage, respectively.

Preparation of Cross-linked PIB Network for Permeation Study. After optimizing the irradiation time from the kinetic study of the photodimerization, a 2 wt % solution of the polymer in THF was taken in 5 cm^2 Teflon mold. The solvent was allowed to evaporate, and the polymer was dried under vacuum at room temperature for 12 h and photo cross-linked using a 400 W high-pressure mercury lamp (Uvitron International, Inc., PORTA-RAY 400 R) for 8 min at λ_{max} = 365 nm (UVA irradiation) to obtain cross-linked polymer sample.

Characterization. *NMR Spectroscopy.* ^{1}H NMR spectra of the synthesized materials were recorded at 25 °C on a Bruker 500 MHz spectrometer using $CDC1_3$ (Cambridge Isotope Lab., Inc.) as the solvent and tetramethylsilane (TMS) as the internal reference (δ H 0.00).

SEC Measurements. The absolute number-average molecular weight (M_n) and molecular weight distribution (M_w/M_n) of the purified polymers were measured by SEC using a Waters model 717 Plus autosampler, a model 515 HPLC pump, a model 2410 differential refractometer, a model 2487 UV−vis detector, an online multiangle laser light scattering (MALLS) detector (MiniDawn, Wyatt Technology, Inc.; measurement angles are 44.7°, 90.0°, and 135.4°), an online differential viscometer (ViscoStar, Wyatt Technology Inc.), and five Styragel HR SEC columns connected in the following order of pore diameters: 500, 10^3, 10^4, 10^5, and 100 Å. RI was the concentration detector. THF was used as the eluent at a flow rate of 1.0 mL min^{-1} at room temperature. The results were processed by the Astra 5.4 software (Wyatt Technology, Inc.).

Matrix-Assisted Laser Desorption/Ionization Time-of-Flight Mass Spectrometry (MALDI-TOF MS). The MALDI-TOF MS measurements were performed with a Bruker BIFLEX III mass spectrometer equipped with a time-of-flight (TOF) mass analyzer. In all cases, 19 kV acceleration voltage was used with pulsed ion extraction (PIETM). The positive ions were detected in the reflectron mode (20 kV). A nitrogen laser (337 nm, 3 ns pulse width, 106−107 W cm^{-2}) operating at 4 Hz was used to produce laser desorption, and 500 shots were summed. The MALDI-TOF MS spectra were externally calibrated with poly(ethylene glycol) standards (M_n = 1450 g mol^{-1} and M_n = 6000 g mol^{-1}) using linear calibration. Samples for MALDI-TOF MS were prepared with dithranol matrix (20 mg mL^{-1}), $(PIB\text{-}MUMB)_3$ (10 mg mL^{-1}) and sodium trifluoroacetate (used as the cationization

DOI: 10.1021/am508096c
ACS Appl. Mater. Interfaces 2015, 7, 2064−2072

Scheme 1. Synthesis of Triarm Star Coumarin Functionalizd PIB

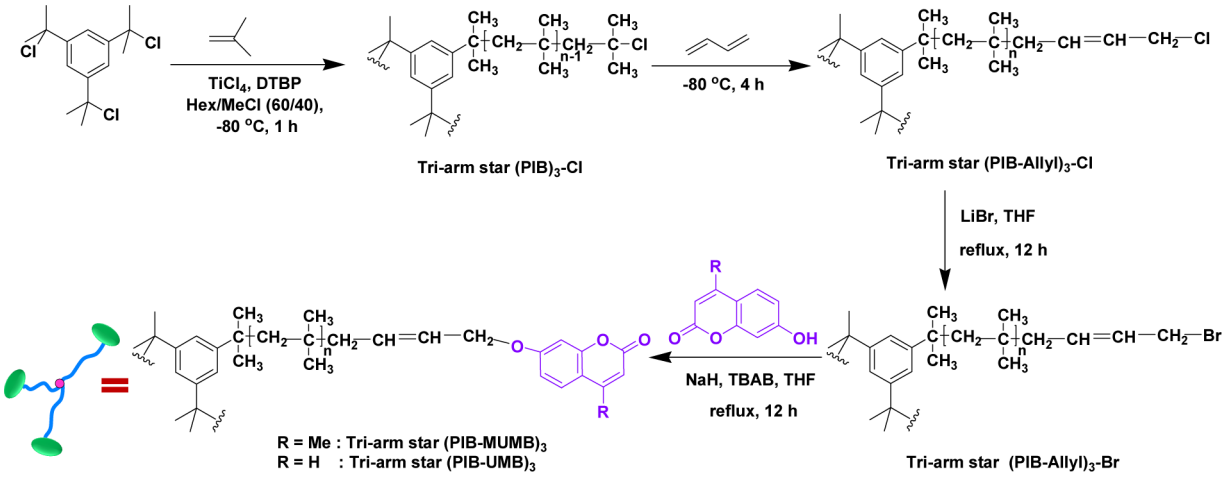

agent, 5 mg mL^{-1}) dissolved in THF. The solutions were mixed in a 8:8:1 (v/v) ratio (matrix/analyte/cationization agent). A volume of 1 μL of the solution was deposited onto a metal sample plate and allowed to air-dry.

Electrospray Quadrupole Time-of-Flight Mass Spectrometry (ESI-Q-TOF MS). The ESI-Q-TOF MS measurements were performed with a MicroTOF-Q type Qq-TOF MS instrument (Bruker Daltoniks, Bremen, Germany) using an ESI source with positive ion mode. The $(PIB\text{-}MUMB)_3$ samples dissolved in THF/methanol mixture of 3:1 (v/v) at a concentration of 1 mg mL^{-1} were introduced directly into the ESI source with a syringe pump (Cole-Parmer, Vernon Hills, IL) at a flow rate of 3 μL min^{-1}. The spray voltage was set to 4 kV. The temperature of the drying gas (N_2) was kept at 180 °C. The mass spectra were calibrated externally using the exact masses of the clusters generated from the electrosprayed solution of sodium trifluoroacetate (NaTFA). The mass spectra recorded were evaluated with the DataAnalysis 3.4 software from Bruker.

UV–Vis Spectroscopic Analysis. UV–vis absorption spectra of the samples were acquired in a Hewlett-Packard 8453 UV–vis spectrophotometer.

Atomic Force Microscopy (AFM) Analysis. AFM study was carried on the polymer thin film spin-coated from THF solution (20 mg mL^{-1}) on silicon wafer followed by drying in vacuum at room temperature for 12 h. It was then photo cross-linked using a 400 W high-pressure mercury lamp (Uvitron International Inc. PORTA-RAY 400 R) at λ_{max} = 365 nm (UVA irradiation) to obtain ~100% cross-linked polymer sample. A rigid Veeco (TESP) Si tip with nominal spring constant, k ~ 42 N m^{-1}, and resonant frequency, f_0 ~ 320 kHz was used to make a scratch on the surface of the polymer film. We adjusted the deflection set point in the Nanoscope software so that the tip was pushed into the film with some positive pressure and scanned along the x axis only, resulting in scratches with depths ranging from hundreds of nanometers to microns. The scratched cross-linked polymer film samples were irradiated with 400 W medium pressure visible lamp (UVC light, λ_{max} = 254 nm) (Intensity 7.5 mW cm^{-2}) and high-power UVA light (Intensity 21 mW cm^{-2}) (λ_{max} = 365 nm) from Uvitron International, Inc. (PORTA-RAY 400 R) or low-power UV lamp (λ_{max} = 365 nm; Spectroline E-Series Ultraviolet hand lamps, Intensity 0.3 mW cm^{-2}). For sunlight-induced self-healing, scratched samples were exposed to sunlight. At time zero, and after various irradiation times, images of the scratch area were obtained in a Veeco Nanoscope IIIa Multimode AFM operating in tapping mode at room temperature. Cross-sectional images and depth profiles were obtained using the Nanoscope software in section analysis mode.

Oxygen Transmission Rate (OTR) Measurements. Oxygen permeability analysis was tested with an Illinois Instruments Oxygen Permeability Analyzer 8001 at 60% relative humidity (RH) and 25 °C. The area of measurement of the samples was 2.5 cm^2. The RH and temperature were instrumentally controlled. The thickness of the film was 0.35 mm. The instrumental setup is based on ASTM D3985. The sample was tested in duplicate.

Water Vapor Transmission Rate (WVTR) Measurements. Water permeability was tested using a MOCON Permatran-W 3/33, in accordance with ASTM F1249 at 25 °C and 60% RH, utilizing 5 cm^2 specimens. The film thickness was 0.35 mm. The sample was tested in duplicate.

RESULTS AND DISCUSSION

Synthesis of Coumarin Functionalized Triarm Star PIBs. The synthetic route of coumarin functionalized triarm star PIB $(PIB\text{-}MUMB)_3$ with number-average molecular weight (M_n) = 2000 g mol^{-1} [$(PIB\text{-}MUMB)_3$-2k], 5000 g mol^{-1} [$(PIB\text{-}MUMB)_3$-5k] and 10000 g mol^{-1} [$(PIB\text{-}MUMB)_3$-10k] is presented in Scheme 1 (see the Experimental Section for the detailed synthesis procedure). To ensure their easy accessibility during intermolecular reactions and facilitate a rapid self-healing process, we introduced the coumarin functionality responsible for self-healing into the periphery of the triarm star polymer. Molecular structures of the polymers were confirmed by ^1H NMR spectroscopy (Figure 1). ^1H NMR spectrum showed the disappearance of peaks at 3.98, 5.68, and 5.79 ppm assigned to the bromomethylene and bromoallylmethine protons and new signals at 4.57, 5.68, and 5.89 ppm assigned to $-CHC\underline{\boldsymbol{H}}_2O-$, $-CH{=}C\underline{\boldsymbol{H}}CH_2O-$ and $-C\underline{\boldsymbol{H}}{=}CHCH_2O-$ appeared, indicating quantitative conversion. New peaks appeared at 2.39 and at 6.82 and 7.48 ppm for $-OCOC\underline{\boldsymbol{H}}-$ and for aromatic signals, respectively, suggesting quantitative conversion. The M_n and molecular weight distribution (M_w/M_n) of the polymers were determined from the SEC analysis (Table 1). The SEC-RI traces of $(PIB\text{-}MUMB)_3$ samples are almost identical to that of $(PIB\text{-}Allyl)_3$-Cl suggesting no change in the polymer backbone during post functionalization reactions (Figure S1, Supporting Information).

Quantitative end functionality of $(PIB\text{-}MUMB)_3$ was confirmed by MALDI-TOF MS. The MALDI-TOF MS spectra of $(PIB\text{-}MUMB)_3$-2k (Figure 2A) and $(PIB\text{-}MUMB)_3$-5k (Figure 2B) show a series of peaks spaced by 56 Da, which corresponds to the mass of an IB unit. Furthermore, as expected, due to the presence of several oxygen atoms in the $(PIB\text{-}MUMB)_3$ derivatives, $(PIB\text{-}MUMB)_3$-s are cationized mostly with sodium ions, that is, $[M + Na]^+$ adduct ions were formed under MALDI-TOF MS conditions. In addition, owing to the ubiquitous presence of potassium ions in the

DOI: 10.1021/am508096c
ACS Appl. Mater. Interfaces 2015, 7, 2064–2072

samples, beside the sodiated ones, the potassiated (PIB-MUMB)$_3$-s also appeared with low intensities in MALDI-TOF MS spectra. The measured masses are in good agreement with those calculated based on the corresponding (PIB-MUMB)$_3$ compositions (Table 1). For example, in Figure 2A the measured and the calculated masses for the sodiated (PIB-MUMB)$_3$ oligomer with a number of IB units (n) = 20 are 2033.8 and 2033.7 Da, respectively (the composition is $C_{137}H_{220}O_9Na$, and the mass is given for the most intensive isotopic peaks, because isotopic resolution was obtained in this mass range). Furthermore, in Figure 2B, the measured and calculated masses for the sodiated (PIB-MUMB)$_3$ oligomer with n = 60 were found to be 4278.9 and 4278.5 Da, respectively (the composition corresponds to $C_{297}H_{540}O_9Na$, and the masses given are the average masses because isotopic resolution could not be achieved in this mass range). However, due to the poor ionization efficiency for the (PIB-MUMB)$_3$-10k, no appreciable MALDI-TOF MS spectrum was obtained. Interestingly, ESI-TOF MS spectrum was successfully obtained for (PIB-MUMB)$_3$-2k, albeit with low signal-to-noise ratio. The ESI-TOF MS spectrum for the (PIB-MUMB)$_3$-2k (Figure S2, Supporting Information) is similar to that obtained by MALDI-TOF MS, except that the ESI-TOF MS spectrum is shifted to lower masses compared to the MALDI-TOF MS spectrum. This finding is most probably due to the more significant decrease of the ESI ionization efficiency with the increasing lengths of the nonpolar PIB chains as compared to that of MALDI. This is supported by the fact that no ESI-TOF MS spectrum could be obtained for the (PIB-MUMB)$_3$-5k or higher. However, we can utilize the much higher mass accuracy and resolution of ESI-TOF MS measurements in the case of (PIB-MUMB)$_3$-2k to compare the measured and calculated masses for the different oligomer peaks. For example, the measured and calculated masses for the sodiated (PIB-MUMB)$_3$ oligomer with n = 20 are 2033.665 and 2033.668 Da, respectively (the composition is $C_{137}H_{220}O_9Na$, and the mass is given for the most intensive isotopic peaks).

Photodimerization/Photocleavage of Coumarin Functionalized Triarm Star PIB. The photodimerization reactions of (PIB-MUMB)$_3$-2k was carried out using UV light of λ_{max} = 365 nm (UVA) (see the Experimental Section for the detailed procedure), and the progress of the photodimerization was monitored by UV−vis spectroscopy. A gradual decrease of absorbance of coumarin at 320 nm with time during photodimerization was observed (Figure 3A), indicating dimerization of coumarin moieties to form a cyclobutane ring. The change in absorbance at 320 nm (A_{320}) values directly reflects the degree of cross-linking of polymers. Hence, the photo cross-linking percentage of the polymer (D) can be approximately estimated from the A_{320} value using the following equation:

$$D = [\{(A_{320})_0 - (A_{320})_t\}/(A_{320})_0] \times 100 \quad (1)$$

where, $(A_{320})_0$ and $(A_{320})_t$ are the absorbance of polymers at 320 nm before and after irradiation for t min, respectively. Maximum cross-linking of the polymer (~95%) could be achieved after UVA irradiation for 8 min (3A, inset), and then it leveled off. With increase in molecular weight of (PIB-MUMB)$_3$ (as in case of (PIB-MUMB)$_3$-5k and (PIB-MUMB)$_3$-10k), the efficiency of photodimerization slightly decreased to ~90% in 8 min (Figure S3, Supporting Information). Thus, we focused our later studies on (PIB-MUMB)$_3$-2k.

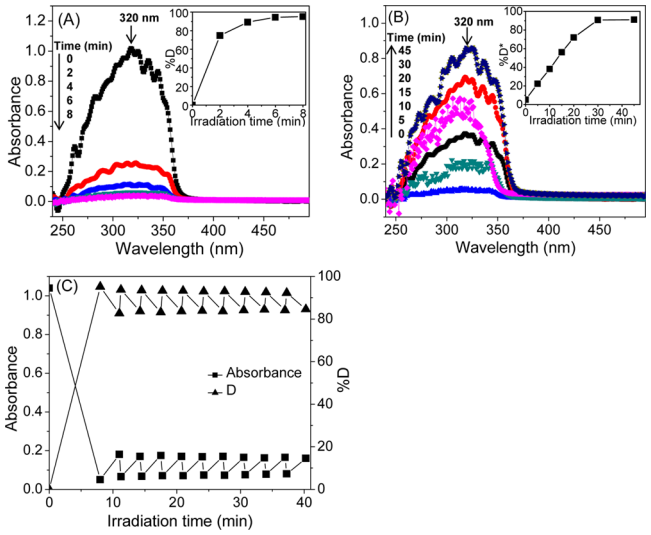

Figure 3. Successive UV−vis absorption spectra of (PIB-MUMB)$_3$-2k thin film during (A) photodimerization upon irradiation with UVA (λ_{max} = 365 nm) for different times and (B) photocleavage upon irradiation with UVC (λ_{max} = 254 nm) for different times; (inset) plot of cross-linking percentage (%D) or cleavage percentage (%D*) vs time of the respective plots. (C) Reversible photodimerization/photocleavage cycle of (PIB-MUMB)$_3$-2k. After initial irradiation with UVA (λ_{max} = 365 nm) for 8 min to prepare the cross-linked network, the film was irradiated with consecutive UVC (λ_{max} = 254 nm) for 3 min and UVA (λ_{max} = 365 nm) for 0.25 min up to 10 cycles.

The photocleavage reactions of cross-linked (PIB-MUMB)$_3$-2k was carried out using UV light of λ_{max} = 254 nm (UVC; see the Experimental Section for the detailed procedure). A gradual increase of absorbance of coumarin at 320 nm with time during photocleavage was observed (Figure 3B), indicating that the cyclobutane ring in the photodimer of coumarin moiety is gradually cleaved to regenerate coumarin. However, a leveling off in the absorbance is observed after irradiation for 30 min for (PIB-MUMB)$_3$. The photo cleavage percentage (D*) is determined by the following equation:

$$D^* = \{(100 - D_t)/D_0)\} \times 100 \quad (2)$$

where D_0 and D_t are the cross-linking percentage when photo cleavage occurs for 0 and t minutes, respectively. The plot of D* values versus UV irradiation time (t; Figure 3B, inset) revealed that the final photo cleavage percentage was 91% after 45 min of photo irradiation. Furthermore, Figure 3 revealed that only part of the photodimer can be reverted back to the starting material. This is probably due to the restricted mobility of the pendant coumarin moieties.[40]

Photoreversibility of Photo Cross-Linked Coumarin Functionalized Triarm Star PIB. Figure 3C depicts the results of the reversibility of the photodimerization/photocleavage cycle of (PIB-MUMB)$_3$-2k utilizing UV−vis spectroscopy. The cross-linked PIB network was prepared by irradiating the film with UVA (λ_{max} = 365 nm) for 8 min. Subsequently, the photoreversibility was studied by irradiating it with UVC (λ_{max} = 254 nm) for 3 min and UVA for 0.25 min up to 10 cycles while keeping the photocleavage at ~15% during the photoreversibility study. The corresponding cross-linking percentages were calculated using eq 1. The photodimerization and photocleavage cycle were repeated 10 times with approximately 89% reversion. The absorbance did not revert quantitatively due to a well-documented equilibrium between

DOI: 10.1021/am508096c
ACS Appl. Mater. Interfaces 2015, 7, 2064−2072

the dimer and cleaved coumarin under irradiation with UVC (λ_{max} = 254 nm).[41,42]

UV-Induced Self-Healing Behavior of Photo Cross-Linked Triarm Star PIB. Self-healing behavior of the photo cross-linked triarm star PIB network films was studied using atomic force microscopy (AFM) in tapping mode. AFM is an established analytical tool to induce a mechanical cut on a surface and to analyze changes of the damage surface.[43]

Mechanical cuts ranging from nm to μm in depth were made in the cross-linked polymer films using commercial silicon tips in contact mode (see Experimental Section for the detailed procedure). Initially, a cut with a depth of 74 nm was made in the cross-linked thin film of the $(PIB\text{-}MUMB)_3$-2k, as analyzed by the tapping mode AFM image (Figure 4A). The damaged

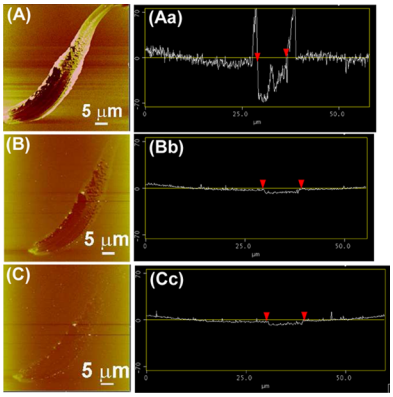

Figure 4. Time-dependent change of height mode AFM image for the cut on the surface of the cross-linked $(PIB\text{-}MUMB)_3$-2k film using a high-powered UV lamp, time = (A) 0, (B) 5, and (C) 30 min. (Aa–Cc) Corresponding depth profiles reveal the evolution of the damage depth.

surface was exposed to consecutive UVC (λ_{max} = 254 nm; 400 W medium-pressure mercury lamp, Uvitron International, Inc., PORTA-RAY 400 R, Intensity 7.5 mw cm^{-2}) and UVA (λ_{max} = 365 nm; 400 W high-pressure mercury lamp, Uvitron International, Inc., PORTA-RAY 400 R, Intensity 21 mw cm^{-2}) irradiation for 5 min. AFM image of the surface after 5 min of exposure to UVC and UVA irradiation revealed that the cut healed up to ~86% as the depth of the cut decreased to 10 nm (Figure 4B). With further exposure to UVC and UVA irradiation for 25 min, the depth of the cut decreased to 5 nm (Figure 4C). A deep cut of 918 nm depth was made in the cross-linked thin film of $(PIB\text{-}MUMB)_3$-2k (Figure 5A) and its self-healing behavior was studied using simultaneous exposure to UVC (λ_{max} = 254 nm) and UVA (λ_{max} = 365 nm) irradiation for 30 min. Tapping mode AFM image of the surface after healing for 30 min revealed 95% healing as the depth of the cut decreased to 41 nm (Figure 5B). Self-healing could be observed, even when a low-intensity UV lamp (intensity, 0.3 mw cm^{-2}) was employed, although the rate was slower (~80% healing in 40 min; Figure S4, Supporting Information).

Sunlight-Induced Self-Healing Behavior of Photo Cross-Linked Triarm Star PIB. The successful study of self-healing of $(PIB\text{-}MUMB)_3$-2k using lower intensity UV lamp prompted us to explore the possibility of healing of the damaged surface under direct sunlight. A 260 nm deep cut was prepared on the cross-linked thin film of $(PIB\text{-}MUMB)_3$-2k (Figure 6A). The damaged surface was exposed to sunlight, and AFM images were recorded at different time intervals. The

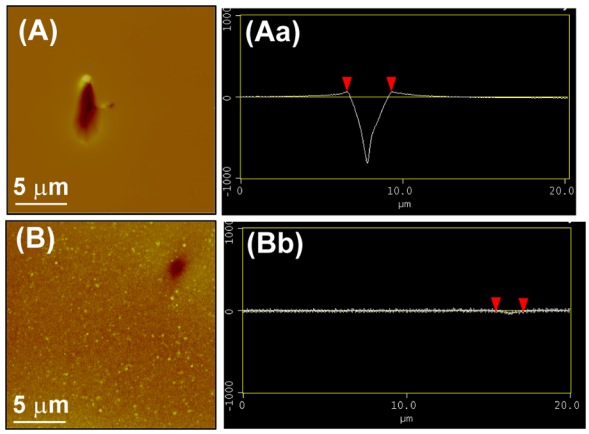

Figure 5. Time-dependent change of height mode AFM image for the cut on the surface of the cross-linked $(PIB\text{-}MUMB)_3$-2k film using high power UV lamp: time = (A) 0 and (B) 30 min. (Aa and Bb) Corresponding depth profiles reveal the evolution of the damage depth.

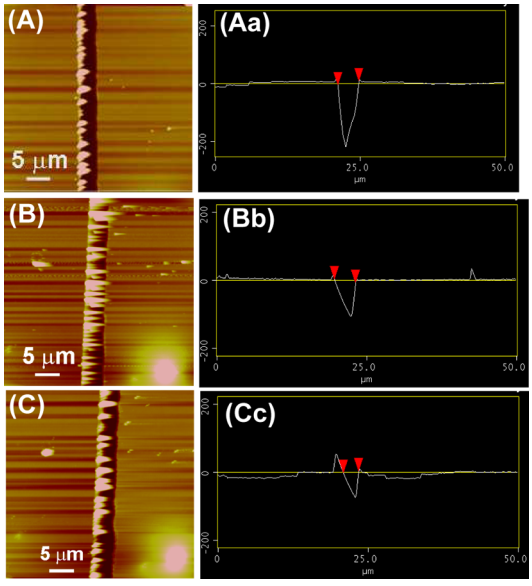

Figure 6. Time-dependent change of height mode AFM image for the cut on the surface of the cross-linked $(PIB\text{-}MUMB)_3$-2k film using sunlight: time = (A) 0, (B) 6, and (C) 12 h. (Aa–Cc) Corresponding depth profiles reveal the evolution of the damage depth.

depth of the cut decreased to 112 and 80 nm (70% healing) after exposure to sun irradiation for 6 and 12 h, respectively (Figure 6B and Figure 6C).

The rate of healing under sunlight was also studied with $(PIB\text{-}UMB)_3$. $(PIB\text{-}UMB)_3$-2k was synthesized with quantitative end-functionality as described in the Experimental Section (Figures S5 and S6, Supporting Information). Results of the reversibility study of the photodimerization/photocleavage cycle of $(PIB\text{-}UMB)_3$-2k (Figure S7, Supporting Information) was found to be close to that of $(PIB\text{-}UMB)_3$-2k (Figure 3C). The rate of healing on cross-linked thin film of the polymer was studied by introducing a cut with a depth of 79 nm (Figure S8A, Supporting Information). Subsequently, the damaged surface was exposed to sunlight, and AFM images were recorded after 6 and 12 h. The cut depth reduced to 36 nm in 6 h and to 24 nm in 12 h (Figure S8B,C, Supporting Information). The healing efficiency for $(PIB\text{-}UMB)_3$ was

DOI: 10.1021/am508096c
ACS Appl. Mater. Interfaces 2015, 7, 2064–2072

Scheme 2. Reversible Cross-Linked Network Formation via Photodimerization/Photocleavage of Coumarin Functionalized Tri-Arm Star PIB and a Possible Mechanism for Self-Healing Process

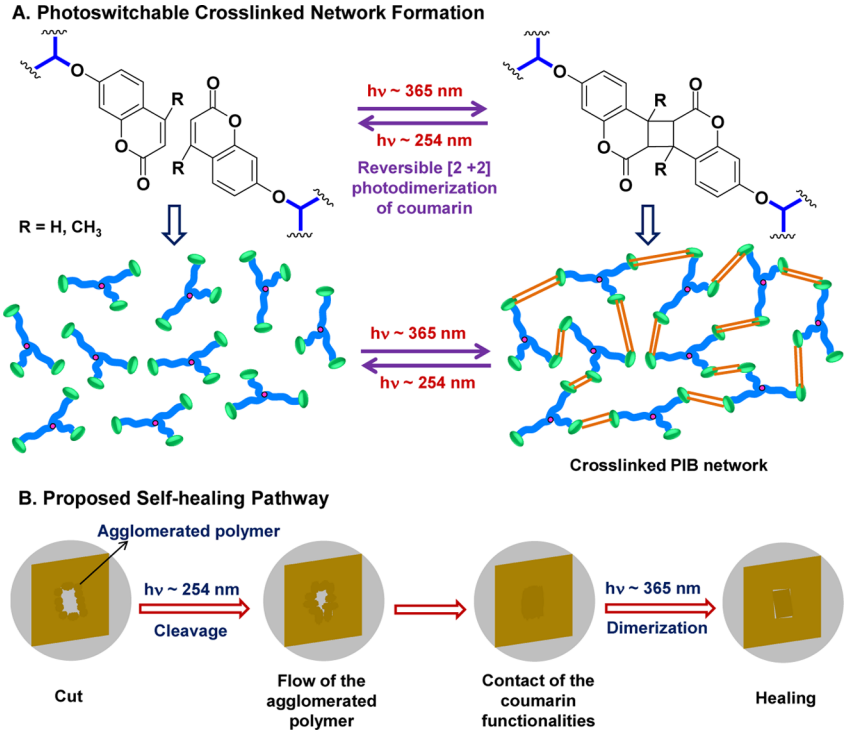

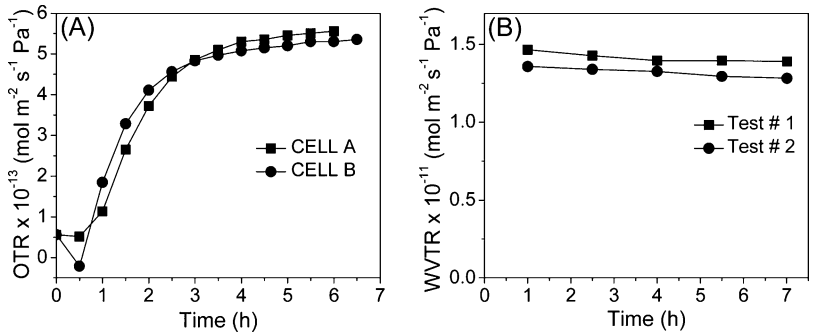

Figure 7. (A) Oxygen transmission rate (OTR) and (B) water vapor transmission rate (WVTR) obtained for the cross-linked $(PIB\text{-}MUMB)_3$-2k film (0.35 mm thick) performed at 25 °C and RH 60%.

calculated to be 70% after 12 h of exposure to sunlight, which is similar to that observed in case of $(PIB\text{-}MUMB)_3$-2k (Figure 6).

Mechanism of Photoinduced Self-Healing of Cross-Linked PIB Network. The role of UVC/UVA-induced reversible cross-linking in the self-healing behavior was examined by comparing the damage induced to a control sample containing permanent cross-linked bonds. A cut of depth 200 nm was introduced in a control sample, as analyzed by tapping mode AFM image (Figure S9A, Supporting Information). It was then protected from light and AFM images were taken after 24 and 48 h. Tapping mode AFM images of the surface after 24 and 48 h (Figure S9B,C, Supporting Information) reveal that there is some reduction of the cut depth: 170 nm (after 24 h) and 150 nm (after 48 h). But, any significant healing was absent in the control sample in the absence of UVC/UVA radiation. The observed slight decrease of the cut depth occurred solely due to the viscoelastic restoration, as observed by earlier researchers.[44]

Detailed analysis of the healing behavior shows that the healing response could be driven by first breaking of the cyclobutane ring via photocleavage induced by UVC allowing the polymer to flow and come closer. The glass transition temperature of PIB is ~ −70 °C.[45,46] Thus, PIB have sufficient mobility to flow at the temperature of the self-healing study (room temperature) allowing the coumarin functionalities to come closer. At this stage reformation of the cyclobutane ring via UVA induced photodimerization allows formation of the cross-linked network which eventually heal the damage (Scheme 2). The piles of agglomerated polymeric material around the edges of the scratch served as the storage of the material that released it back to the cuts and facilitated the healing process. Generally, macroscopic fusion of a cross-linked polymer in the bulk state is hindered due to the limited chain mobility.[47] Thus, it is not possible for the cut surfaces to come in full contact with each other.

Permeability Analysis of the Photo Cross-Linked Triarm Star PIB Film. Figure 7 presents duplicate result of

DOI: 10.1021/am508096c
ACS Appl. Mater. Interfaces 2015, 7, 2064−2072

oxygen permeation rate (OTR) analysis and water vapor transmission rate (WVTR) analysis, respectively, of the cross-linked thin film (film thickness = 0.35 mm) of (PIB-MUMB)$_3$-2k. Permeability studies revealed OTR value of 5.5×10^{-13} mol m^{-2} s^{-1} Pa^{-1} or oxygen permeability of 1.9×10^{-16} mol m m^{-2} s^{-1} Pa^{-1} and WVTR value of 1.3×10^{-11} mol m^{-2} s^{-1} Pa^{-1} or moisture permeability of 46×10^{-16} mol m m^{-2} s^{-1} Pa^{-1}. The low permeability of oxygen and water vapor of the cross-linked network might be attributed to the presence of bulky methyl groups in its IB component.[48] Importantly, PIB-based self-healing sealant possess much lower moisture permeability compared to previously reported sealants such as Emmerson-Cummins semiflexible sealant [$(100-200) \times 10^{-16}$ mol m m^{-2} s^{-1} Pa^{-1}]; highly flexible sealant [$(212-499) \times 10^{-16}$ mol m m^{-2} s^{-1} Pa^{-1}]; DELO flexible sealant [$(1267-4753) \times 10^{-16}$ mol m m^{-2} s^{-1} Pa^{-1}]; and silyl terminated polyacrylate polymer (634×10^{-16} mol m m^{-2} s^{-1} Pa^{-1}).[49]

CONCLUSIONS

Coumarin functionalized PIB triarm star polymers with quantitative functionality could be prepared by a simple nucleophilic substitution of bromoallyl-trifunctional PIB with 4-methylumbelliferone or umbelliferone in the presence of NaH. The coumarin functionalized PIB triarm star polymers undergo rapid and efficient cross-linking upon irradiation with UV light at λ_{max} = 365 nm. Photocleavage can be affected by irradiation with UV light at λ_{max} = 254 nm, and the photodimerization/photocleavage cycle can be repeated multiple times without the deterioration of the healing ability. Healing of damage takes place even under sunlight, albeit more slowly. The cross-linked PIB films exhibit excellent barrier property against oxygen and moisture, which makes them potentially useful as coating for photovoltaic devices.

ASSOCIATED CONTENT

Supporting Information

Additional analytical analysis including spectral data. This material is available free of charge via the Internet at http://pubs.acs.org.

AUTHOR INFORMATION

Corresponding Author

*E-mail: Rudolf_Faust@uml.edu.

Notes

The authors declare no competing financial interest.

ACKNOWLEDGMENTS

The authors thank Dr. Daniel Schmidt, University of Massachusetts Lowell for the oxygen permeability analysis and Sarah Cheney, U.S. Army NSRDEC for assistance in acquiring the water vapor transmission analysis data. Financial support from Commercial Ventures and Intellectual Property (CVIP), University of Massachusetts Lowell is greatly appreciated (R.F.). This work was also supported by the European Union and the State of Hungary, cofinanced by the European Social Fund, in the framework of TÁMOP-4.2.4.A/2-11/1-2012-0001 National Excellence Program (S.K.) and the grant OTKA K 101850.

REFERENCES

(1) White, S. R.; Sottos, N. R.; Geubelle, P. H.; Kessler, M. R.; Sriram, S. R.; Brown, E. N.; Viswanathan, S. Autonomic Healing of Polymer Composites. *Nature* **2001**, *409*, 794−797.
(2) Cho, S. H.; Andersson, H. M.; White, S. R.; Sattos, N. R.; Braun, P. V. Polydimethylsiloxane-based Self-Healing Materials. *Adv. Mater.* **2006**, *18*, 997−1000.
(3) Rule, J. D.; Sottos, N. R.; White, S. R. Effect of Microcapsule Size on the Performance of Self-Healing Polymers. *Polymer* **2007**, *48*, 3520−3529.
(4) Pratama, P. A.; Sharifi, M.; Peterson, A. M.; Palmese, G. R. Room Temperature Self-Healing Thermoset Based on the Diels−Alder Reaction. *ACS Appl. Mater. Interfaces* **2013**, *5*, 12425−12431.
(5) Habault, D.; Zhang, H.; Zhao, Y. Light-Triggered Self-Healing and Shape-Memory Polymers. *Chem. Soc. Rev.* **2013**, *42*, 7244−7256.
(6) Otsuka, H.; Aotani, K.; Higaki, Y.; Amamoto, Y.; Takahara, A. Thermal Reorganization and Molecular Weight Control of Dynamic Covalent Polymers Containing Alkoxyamines in Their Main Chains. *Macromolecules* **2007**, *40*, 1429−1434.
(7) Sheridan, R. J.; Bowman, C. N. Understanding the Process of Healing of Thermoreversible Covalent Adaptable Networks. *Polym. Chem.* **2013**, *4*, 4974−4979.
(8) Kowalski, D.; Ueda, M.; Ohtsuka, T. Self-Healing Ion-Permselective Conducting Polymer Coating. *J. Mater. Chem.* **2010**, *20*, 7630−7633.
(9) Chuo, T.-W; Wei, T.-C.; Liu, Y.-L. Electrically Driven Self-Healing Polymers Based on Reversible Guest−Host Complexation of β-Cyclodextrin and Ferrocene. *J. Polym. Sci. A Polym. Chem.* **2013**, *51*, 3395−3403.
(10) Schultz, R. K.; Myers, R. R. The Chemorheology of Poly(vinyl alcohol)−Borate Gels. *Macromolecules* **1969**, *2*, 281−285.
(11) Wang, Z.; Urban, M. W. Facile UV-Healable Polyethylenimine−Copper (C_2H_5N−Cu) Supramolecular Polymer Networks. *Polym. Chem.* **2013**, *4*, 4897−4901.
(12) Bode, S.; Zedler, L.; Schacher, F. H.; Dietzek, B.; Schmitt, M.; Popp, J.; Hager, M. D.; Schubert, U. S. Self-Healing Polymer Coatings based on Crosslinked Metallosupramolecular Copolymers. *Adv. Mater.* **2013**, *25*, 1634−1638.
(13) Maeda, T.; Otsuka, H.; Takahara, A. Dynamic Covalent Polymers: Reorganizable Polymers with Dynamic Covalent Bonds. *Prog. Polym. Sci.* **2009**, *34*, 581−604.
(14) Yuan, C.; Rong, M. Z.; Zhang, M. Q.; Zhang, Z. P.; Yuan, Y. C. Self-Healing of Polymers via Synchronous Covalent Bond Fission/Radical Recombination. *Chem. Mater.* **2011**, *23*, 5076−5081.
(15) Chen, Y.; Kushner, A. M.; Williams, G. A.; Guan, Z. Multiphase Design of Autonomic Self-Healing Thermoplastic Elastomers. *Nat. Chem.* **2012**, *4*, 467−472.
(16) Vidyasagar, A.; Handore, K.; Sureshan, K. M. Soft Optical Devices from Self-Healing Gels Formed by Oil and Sugar-Based Organogelators. *Angew. Chem., Int. Ed.* **2011**, *50*, 8021−8024.
(17) Wang, Q.; Mynar, J. L.; Yoshida, M.; Lee, E.; Lee, M.; Okuro, K.; Kinbara, K.; Aida, T. High-Water-Content Mouldable Hydrogels by Mixing Clay and a Dendritic Molecular Binder. *Nature* **2010**, *463*, 339−343.
(18) Kalista, S. J.; Ward, T. C. Thermal Characteristics of the Self-Healing Response in Poly(ethylene-co-methacrylic acid) Copolymers. *J. R. Soc., Interface* **2007**, *4*, 405−411.
(19) Hansen, M. R.; Graf, R.; Sekharan, S.; Sebastiani, D. Columnar Packing Motifs of Functionalized Perylene Derivatives: Local Molecular Order Despite Long-Range Disorder. *J. Am. Chem. Soc.* **2009**, *131*, 5251−5256.
(20) Burattini, S.; Greenland, B. W.; Merino, D. H.; Weng, W.; Seppala, J.; Colquhoun, H. M.; Hayes, W.; Mackay, M. E.; Hamley, I. W.; Rowan, S. J. A Healable Supramolecular Polymer Blend Based on Aromatic π−π Stacking and Hydrogen-Bonding Interactions. *J. Am. Chem. Soc.* **2010**, *132*, 12051−12058.
(21) Liu, Y.-L.; Chuo, T.-W. Self-Healing Polymers based on Thermally Reversible Diels−Alder Chemistry. *Polym. Chem.* **2013**, *4*, 2194−2205.

DOI: 10.1021/am508096c
ACS Appl. Mater. Interfaces 2015, 7, 2064−2072

(22) Chung, C.-M.; Roh, Y.-S.; Cho, S.-Y.; Kim, J.-G. Crack Healing in Polymeric Materials via Photochemical [2 + 2] Cycloaddition. *Chem. Mater.* **2004**, *16*, 3982−3984.
(23) Trenor, S. R.; Long, T. E.; Love, B. J. Photoreversible Chain Extension of Poly(ethylene glycol). *Macromol. Chem. Phys.* **2004**, *205*, 715−723.
(24) Nagata, M.; Yamamoto, Y. Synthesis and Characterization of Photocrosslinked Poly(ε-caprolactone)s Showing Shape-Memory Properties. *J. Polym. Sci., Part A-1: Polym. Chem.* **2009**, *47*, 2422−2433.
(25) Nagata, M.; Yamamoto, Y. Photocurable Shape-Memory Copolymers of ε-Caprolactone and L-Lactide. *Macromol. Chem. Phys.* **2010**, *211*, 1826−1835.
(26) Nagata, M.; Sato, Y. Synthesis and Properties of Photocurable Biodegradable Multiblock Copolymers Based on Poly(ε-caprolactone) and Poly(L-lactide) Segments. *J. Polym. Sci., Part A-1: Polym. Chem.* **2005**, *43*, 2426−2439.
(27) Forrest, S. R. The Path to Ubiquitous and Low-Cost Organic Electronic Appliances on Plastic. *Nature* **2004**, *428*, 911−918.
(28) Brabec, C. J.; Sariciftci, N. S.; Hummelen, J. C. Plastic Solar Cells. *Adv. Funct. Mater.* **2001**, *11*, 15−26.
(29) Gaume, J.; Wong-Wah-Chung, P.; Rivaton, A.; Therias, S.; Gardette, J.-L. Photochemical Behavior of PVA as an Oxygen-Barrier Polymer for Solar Cell Encapsulation. *RSC Adv.* **2011**, *1*, 1471−1481.
(30) Elowe, P. R.; Stempki, M. A.; Rozeveld, S. J.; DeGroot, M. W. Development of Direct Cell Inorganic Barrier Film Technology providing Exceptional Device Stability for CIGS Solar Cells. *Chem. Mater.* **2011**, *23*, 3915−3920.
(31) Krajewski, T.; Hardikar, K. Protective Layers for a Glass Barrier in a Photovoltaic Device. U.S. Patent US20110315208 A1, Dec 29, 2011.
(32) Ackermann, J.; Schwager, F. Weather-Resistant Backing Films. U.S. Patent CA2806311 A1, Jan 26, 2012.
(33) Chwang, A. B.; Rothman, M. A.; Mao, S. Y.; Hewitt, R. H.; Weaver, M. S.; Silvernail, J. A.; Rajan, K.; Hack, M.; Brown, J. J.; Chu, X.; Moro, L.; Krajewski, T.; Rutherford, N. Thin Film Encapsulated Flexible Organic Electroluminescent Displays. *Appl. Phys. Lett.* **2003**, *83*, 413−415.
(34) Jorgensen, M.; Norrman, K.; Krebs, F. C. Stability/Degradation of Polymer Solar Cells. *Sol. Energy Mater. Sol. C* **2008**, *92*, 686−714.
(35) Sezi, R. Method for Producing a Porous Coating. U.S. Patent US7273821 B2, Sep 25, 2007.
(36) Messe, L.; Chapelat, C. Curable Composition. U.S. Patent WO 2008110564, Sep 18, 2008.
(37) Sherman, M. A.; Kennedy, J. P. Novel Polyisobutylene/poly(dimethylsiloxane) Bicomponent Networks. I. Synthesis and Characterization. *J. Polym. Sci., Part A-1: Polym. Chem.* **1998**, *36*, 1891−1899.
(38) De, P.; Faust, R. Relative Reactivity of C4 Olefins toward the Polyisobutylene Cation. *Macromolecules* **2006**, *39*, 6861−6870.
(39) Higashihara, T.; Feng, D.; Faust, R. Synthesis of Poly(isobutylene-block-methyl methacrylate) by a Novel Coupling Approach. *Macromolecules* **2006**, *39*, 5275−5279.
(40) Motoyanagi, J.; Nishimura, I.; Minoda, M. Living Cationic Polymerization of a Coumarin-Substituted Vinyl Ether and Reversible Photoinduced Crosslinking of the Resulting Homopolymers and Amphiphilic Block Copolymers. *J. Polym. Sci., Part A-1: Polym. Chem.* **2011**, *49*, 4701−4707.
(41) Mal, N. K.; Fujiwara, M.; Tanaka, Y. Photocontrolled Reversible Release of Guest Molecules from Coumarin-Modified Mesoporous Silica. *Nature* **2003**, *421*, 350−353.
(42) Chen, Y.; Chou, C.-F. Reversible Photodimerization of Coumarin Derivatives dispersed in Poly(Vinyl Acetate). *J. Polym. Sci., Part A-1: Polym. Chem.* **1995**, *33*, 2705−2714.
(43) Yufa, N. A.; Li, J.; Sibener, S. J. Diblock Copolymer Healing. *Polymer* **2009**, *50*, 2630−2634.
(44) Yoon, J. A.; Kamada, J.; Koynov, K.; Mohin, J.; Nicolay, R.; Zhang, Y.; Balazs, A. C.; Kowalewski, T.; Matyjaszewski, K. Self-Healing Polymer Films Based on Thiol−Disulfide Exchange Reactions and Self-Healing Kinetics Measured Using Atomic Force Microscopy. *Macromolecules* **2012**, *45*, 142−149.
(45) Malhotra, S. L.; Minh, L.; Blanchard, L. P. Thermal Decomposition and Glass Transition Temperature of Polyisobutylene. *J. Macromol. Sci., Chem.* **1982**, *A18*, 455−475.
(46) Dejean de la Batie, R.; Lauprgtre, F.; Monnerie, L. Carbon-13 NMR Investigation of Local Dynamics in Bulk Polymers at Temperatures Well above the Glass-Transition Temperature. 4. Polyisobutylene. *Macromolecules* **1989**, *22*, 2617−2622.
(47) Amamoto, Y.; Kamada, J.; Otsuka, H.; Takahara, A.; Matyjaszewski, K. Repeatable Photoinduced Self-Healing of Covalently Cross-Linked Polymers through Reshuffling of Trithiocarbonate Units. *Angew. Chem., Int. Ed.* **2011**, *50*, 1660−1663.
(48) Iyengar, Y. Relation of Water Vapor Permeability of Elastomers to Molecular Structure. *J. Polym. Sci., Part B: Polym. Lett.* **1965**, *3*, 663−669.
(49) Grommesh, R. C.; Palmer, R. A.; Zurn, B. J. Dual Seal Photovoltaic Assembly and Method. U.S. Patent US20090194147 A1, Aug 6, 2009.

DOI: 10.1021/am508096c
ACS Appl. Mater. Interfaces 2015, 7, 2064−2072